DTU Library

Identification of potential drug targets in Salmonella enterica sv. Typhimurium using metabolic modelling and experimental validation

Hartman, Hassan B.; Fell, David A.; Rossell, Sergio; Jensen, Peter Ruhdal; Woodward, Martin J.; Thorndahl, Lotte; Jelsbak, Lotte; Elmerdahl Olsen, John ; Raghunathan, Anu; Daefler, Simon

Total number of authors:
11

Link back to DTU Orbit

Editor's Choice

Identification of potential drug targets in *Salmonella enterica* sv. Typhimurium using metabolic modelling and experimental validation

Hassan B. Hartman,[1] David A. Fell,[1] Sergio Rossell,[2]† Peter Ruhdal Jensen,[2] Martin J. Woodward,[3] Lotte Thorndahl,[4] Lotte Jelsbak,[4] John Elmerdahl Olsen,[4] Anu Raghunathan,[5]‡ Simon Daefler[5] and Mark G. Poolman[1]

Correspondence
Mark G. Poolman
mgpoolman@brookes.ac.uk

[1]Department of Medical and Biological Sciences, Oxford Brookes University, Gipsy Lane, Headington, Oxford OX3 OBP, UK

[2]Department of Systems Biology, Technical University of Denmark, Lyngby, Denmark

[3]Department of Food and Nutritional Sciences, University of Reading, Reading, UK

[4]Department of Veterinary Disease Biology, University of Copenhagen, Copenhagen, Denmark

[5]Department of Infectious Diseases, Mount Sinai School of Medicine, New York, NY, USA

Salmonella enterica sv. Typhimurium is an established model organism for Gram-negative, intracellular pathogens. Owing to the rapid spread of resistance to antibiotics among this group of pathogens, new approaches to identify suitable target proteins are required. Based on the genome sequence of *S.* Typhimurium and associated databases, a genome-scale metabolic model was constructed. Output was based on an experimental determination of the biomass of *Salmonella* when growing in glucose minimal medium. Linear programming was used to simulate variations in the energy demand while growing in glucose minimal medium. By grouping reactions with similar flux responses, a subnetwork of 34 reactions responding to this variation was identified (the *catabolic core*). This network was used to identify sets of one and two reactions that when removed from the genome-scale model interfered with energy and biomass generation. Eleven such sets were found to be essential for the production of biomass precursors. Experimental investigation of seven of these showed that knockouts of the associated genes resulted in attenuated growth for four pairs of reactions, whilst three single reactions were shown to be essential for growth.

INTRODUCTION

An urgent concern regarding the treatment of bacterial infection is the development of resistance to existing antibiotics (Paterson, 2006), coupled with the decreased rate of development of new antibiotics. There is therefore a clear need for new approaches to identify novel bacterial targets for drug development (Norrby *et al.*, 2005).

Salmonella enterica sv. Typhimurium is an important cause of food-borne infection and a model organism for other Gram-negative pathogens, notably *S. enterica* sv. Typhi. In the case of *Salmonella*, systemic infection requires that the route for cell invasion, replication and proliferation is via phagocytic and antigen-presenting cells (Prost *et al.*, 2007), and rapid growth of *S.* Typhimurium is seen typically during infection of macrophages. However, there is accumulating evidence for the occurrence of cells entering a metabolically dormant state during infection of cultured fibroblasts (Cano *et al.*, 2003), similar to that of mycobacteria (Murphy & Brown, 2007; García-del Portillo *et al.*, 2008). Observations from animal tissue indicate a total of two or three intracellular replications *in vivo* (Tierrez & García-del Portillo, 2005).

Although many existing antibiotics inhibit enzymic processes, most of these are involved in polymer synthesis, rather than in central carbon metabolism. Sulphonamides

and trimethoprim target biosynthesis of the essential biomass component tetrahydrofolic acid, whereas most other enzyme targets are involved in the synthesis of protein (e.g. aminoglycosides, oxazolidinones, chloramphenicol), RNA (e.g. rifampicin), DNA (e.g. quinolones) or peptidoglycan (e.g. β-lactams, glycopeptides). Enzymes in central carbon metabolism therefore represent an underexplored area in which new antimicrobial drug targets might be identified. In the case of pathogens with access to a wide variety of biomass precursors from their host, uptake of materials from their immediate environment may circumvent the need for *de novo* biosynthesis of these precursors, but central carbon metabolism will still be required to maintain energy and redox balances.

Studies in *S.* Typhimurium have highlighted a major problem associated with identifying metabolic targets in central metabolism, as the bacterium shows excessive network redundancy (Becker *et al.*, 2006), i.e. if a reaction is removed from the network then other routes remain that are able to fulfil or bypass the role. This issue can be addressed by the application of metabolic modelling. In this paper, we combine a number of computational approaches to identify sets of reactions in *S.* Typhimurium whose joint inhibition will abolish or impair the ability to produce biomass precursors by disrupting ATP regeneration and we demonstrate by growth experiments which of the reactions essential *in silico* are also essential *in vitro*.

Respiratory ATP generation has previously been considered as a drug target for *Mycobacterium tuberculosis*. After infection of human macrophages, *M. tuberculosis* can enter a state of dormancy where no or little growth occurs (Wayne & Sohaskey, 2001). Despite the reduced metabolic activity and cellular ATP levels during dormancy, uncouplers of respiratory ATP generation have a strong antimicrobial effect on dormant cells *in vitro* (Rao *et al.*, 2008). Moreover, drug candidates have been developed that specifically inhibit mycobacterial homologues of type II NADH dehydrogenase (phenothiazines and analogous compounds) (Weinstein *et al.*, 2005) and ATP synthase (diarylquinolines) (Andries *et al.*, 2005), indicating the feasibility of targeting a conserved metabolic pathway.

Three genome-scale models (GSMs) of *S.* Typhimurium have been published previously (AbuOun *et al.*, 2009; Raghunathan *et al.*, 2009; Thiele *et al.*, 2011), although they are not entirely independent of one another. The first two were both derived from a previous model of *Escherichia coli*, and the third was generated as a consensus model of the first model and a previously unpublished *S.* Typhimurium model. However, for our purpose, it was convenient to build a model that was based on a publicly available and standardized biochemical database, BioCyc (Karp *et al.*, 2002), as we could then arrive at a model: (i) that was derived directly from an annotated genome, (ii) in which the associations between genes, enzymes and reactions could be identified readily, (iii) where reactions could be compared directly with the many (~2000 at time

of writing) other organisms represented in BioCyc, and (iv) which could be modified rapidly to model metabolic variations amongst other sequenced *Salmonella* strains.

METHODS

Model construction. The model was constructed in a modular fashion using techniques described previously (Poolman *et al.*, 2009, 2013), resulting in a model consisting of: (i) a top-level module, the prime function of which was to import the other modules, (ii) automatically generated reactions, (iii) transport reactions importing nutrients and exporting biomass components and metabolic byproducts, (iv) electron transport chain, and (v) additional and modified reactions. Overall, the model defined a metabolic network capable of generating all biomass components from a minimal medium, consisting of glucose, NH_3, P_i, SO_4 and O_2.

Automatically generated reactions. The BioCyc flat-files corresponding to 'Salmonella enterica enterica serovar Typhimurium str. LT2' were obtained from the BioCyc ftp site (McClelland *et al.*, 2001; Karp *et al.*, 2002). Reactions were generated automatically by extracting reaction and metabolite identifiers and reaction stoichiometries from the flat-files. Reactions involved with non-metabolic species (e.g. 'Damaged-DNA-Pyrimidine') or generic compounds (e.g. 'Aromatic-Oxoacids') were removed, and the atomic balance, in terms of C, N, P and S, was verified for those reactions whose reacting species were associated with an empirical formula in the database.

Transport reactions. The transport module defined all reactions involving transfer between the organism and the environment (with the exception of protons – see below). These were defined with the external species on the left-hand side of the reaction equation, ensuring that all subsequent flux values could be interpreted consistently as positive flux representing transport into the system and negative flux as loss from the system. A transporter was defined for each of the nutrients, and for the metabolic byproducts CO_2, lactate, acetate, succinate, ethanol, formate and methylthioribose [a byproduct of spermidine synthesis, known to be excreted by *E. coli* (Hughes, 2006)].

Generation of biomass was represented by a set of independent transporters, one for each biomass component: protein (as individual amino acids), LPSs, peptidoglycan, membrane, and DNA and RNA (as separate bases) (see Table S1, available in the online Supplementary Material).

Electron transport chain. In general, protons were treated as boundary metabolites. However, they could not be so treated for the reactions of the electron transport chain; here, protons had to be balanced. To this end a separate module was constructed and used to represent the reactions of the electron transport chain. The module defined a system that was capable of synthesizing ATP with the net stoichiometry:

$$4NADH + 9H_i^+ + 2O_2 + 5ADP + 5P_i \rightarrow 4NAD + 9H_2O + 5ATP$$
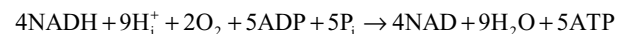
i.e. the oxidation of four molecules of NADH, coupled with the pumping of nine internal H^+, results in the phosphorylation of five ADP to ATP. This corresponds to a P/O ratio of 1.25, which compares to a reported value of 1.33 for *E. coli* (Maloney, 1987). The latter figure is slightly higher as it includes substrate-level phosphorylation.

Miscellaneous reactions. The model contained a small number of reactions that did not fall conveniently into the previous categories.

These included a lumped reaction corresponding to a fatty acid synthetase producing palmitate (then used as a proxy substrate for other reactions that consume fatty acid):

$$8AcCoA + 14NADPH + 7ATP \rightarrow$$
$$palmitate + 14NADP + 8CoA + 7ADP + 7P_i$$
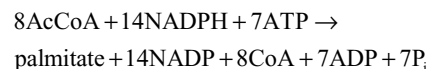
and generic reactions redefined to use specific equivalents. For example, the generic NTP (nucleoside triphosphate) pyrophosphatase:

$$NTP + H_2O \rightarrow NMP + PP_i$$
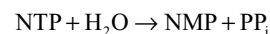
was replaced with four specific reactions, one for each nucleoside base. Reactions that were required for biomass synthesis, but not included in the BioCyc database, were also defined in this section after confirming the presence of the genes encoding the corresponding enzymes (see Table S2).

Model analysis.

Elemental balancing and stoichiometric consistency. For reactions for which the empirical formula of all metabolites are known, determining the net elemental balance is trivial. However, there are instances of reactions, in particular those that involve polymeric reactants, where this is not the case. Although it is then not possible to verify the elemental balance of a single reaction, it is possible to identify sets of such reactions that are defined so as to potentially violate mass conservation (Gevorg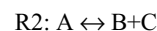yan *et al.*, 2008). The details of the method are beyond the scope of the current paper, but it is predicated on the simple observations that for two reactions R1 and R2 with stoichiometries:

$$R1: A \leftrightarrow B$$

and

$$R2: A \leftrightarrow B+C$$

both cannot be correct and that it is possible to combine both reactions to produce C from nothing, and metabolites A, B and C are referred to as an unconserved set. In the current work, we assumed that water was present to excess, and that it was acceptable for metabolites composed entirely of O and H atoms (with the exceptions of protons pumped by the electron transport chain) to be unconserved.

Enzyme subsets. An enzyme subset is defined as a set of two or more reactions that must carry flux in a fixed ratio in any steady-state flux distribution (Pfeiffer *et al.*, 1999). Such sets are readily determinable from the null-space of the system. In this contribution, the technique is used for two purposes: (i) subsets which involve two or more irreversible reactions defined in opposing directions can carry no steady-state flux and represent a potential error in the model definition, and (ii) they provide a useful technique for condensing a system of reactions, as each subset can be replaced with a single reaction with the net stoichiometry of that subset (see Figs 2 and 3).

Examination of the null-space also allows for the identification of reactions that are not part of inconsistent subsets, but nonetheless cannot carry flux at steady state (*dead* reactions). It is possible that this may underestimate the total (Poolman *et al.*, 2009), but nonetheless identifies the minimum number of dead reactions in a system.

Flux balance analysis (FBA)/linear programming (LP). The application of LP to metabolic models was first described in the 1980s (Fell & Small, 1986; Watson, 1986), further developed in the 1990s as FBA (Varma & Palsson, 1993a, b), and applied subsequently in an ever-increasing variety of ways (Zomorrodi *et al.*, 2012) including to genome-scale networks (Edwards & Palsson, 2000). In its application as FBA it will always include the steady-state assumption as defined by equation 1, and include upper and/or lower bounds on the rates of at least some reactions in the network, where the upper bound can be interpreted as the maximum flux capacity of a reaction. Common objective functions include maximization of the yield of biomass or ATP (Varma & Palsson, 1993b), or minimization of all fluxes (Holzhütter, 2004, 2006), and the latter approach was used here:

$$\text{minimize} : |\mathbf{v}| \quad \text{(objective function)}$$
$$\text{subject to} \begin{cases} \mathbf{Nv=0} \quad \text{(steady state)} \\ v_j = t_j;\ 0 \le j \le X \text{ (biomass production)} \end{cases} \quad (1)$$

i.e. the sum of all fluxes is to be minimized subject to the steady-state constraint (no metabolites are allowed to accumulate) and producing the X biomass precursors at a rate determined by their relative abundance specified in the vector $\mathbf{t}$, which collects the experimentally determined concentrations of all major biomass components (summarized in Table S1), multiplied by a growth rate. Assuming reactions v_0 to v_X are the transporters of the biomass components, biomass production is modelled by fixing each transporter of a biomass component to the corresponding element in $\mathbf{t}$.

Energetic consistency. It is possible that a model that conforms to the consistency tests described above may still violate the law of energy conservation as a result of reactions with incorrectly defined directionality or reversibility leading to cycles that can generate ATP [or NAD(P)H] with no net consumption of substrate. Equation 1 can be modified conveniently to test for such conditions:

$$\text{minimize} : |\mathbf{v}|$$
$$\text{subject to} \begin{cases} \mathbf{Nv=0} \\ v_{\text{ATPase}} = 1 \\ v_j = t_j;\ 0 \le j \le Y \end{cases}$$

where v_{ATPase} represents the flux in an arbitrary ATPase reaction and Y is the number of all transporters (not just those producing biomass components). Any possible solution represents an energetic inconsistency, and reactions therein examined and the model consequently corrected.

Identification of the catabolic core. Our general strategy for identifying novel antimicrobial drug targets is based upon the assumption that abolition or reduction of ATP regeneration will either be fatal or at least reduce virulence. In order to achieve this, we identify a set of reactions that respond to changes in demand for ATP, which we denote the *catabolic core*.

The LP of equation 1 was modified to include an additional constraint representing a demand for ATP:

$$\text{minimize} : |\mathbf{v}|$$
$$\text{subject to} \begin{cases} \mathbf{Nv=0} \\ v_j = t_j;\ 0 \le j \le X \\ v_{\text{ATPase}} = \text{ATPase}; \\ \quad \text{ATPase}_{\min} \le \text{ATPase} \le \text{ATPase}_{\max} \end{cases} \quad (2)$$

The catabolic core can then be identified by solving equation 2 for a range of values of v_{ATPase} and identifying those reactions whose rates

changed in the solution. The lower limit, ATPase$_{min}$, was calculated from the equation:

$$r_{ATP} = Y_{ATP} \cdot \mu + m_{ATP} \qquad (3)$$

using measurements from *E. coli* (Bauchop & Elsden, 1960; Feist *et al.*, 2007): Y_{ATP}=60 mmol ATP gDW^{-1}, m_{ATP}=8.4 mmol ATP (gDW h)$^{-1}$ and μ_{max}=0.91 h^{-1}, which yields a value of ATPase$_{min}$=63 mmol ATP (gDW h)$^{-1}$ (where DW indicates dry weight).

The upper limit, ATPase$_{max}$, was chosen arbitrarily as a value beyond which all responding reactions change linearly. This was found to be 200 mmol ATP (gDW h)$^{-1}$.

Analysis of the catabolic core. Flux values of reactions in the catabolic core, as obtained above, were visualized with a dendrogram, here referred to as a correlation tree, as described in Poolman *et al.* (2007, 2009).

Minimal cut sets (MCSs) (Klamt & Gilles, 2004) of size one, two and three that inhibit ATP production in the catabolic core were identified by repeatedly solving:

$$\text{minimize} \quad : \quad |\mathbf{v}|$$

$$\text{subject to} \quad \begin{cases} \mathbf{Nv=0} \\ v_{ATPase} = r_{ATP} \\ v_i, v_j, v_k = 0;\ i, j, k \in \{1 \dots n\} \end{cases} \qquad (4)$$

where v_i, v_j and v_k are candidate reactions for a new cut set, and ATP demand was fixed at r_{ATP}=63 mmol ATP gDW^{-1}.

The effect of removing each reaction in a cut set from the whole model was determined by constraining their fluxes to zero in equation 1. This analysis was repeated on the three other *S.* Typhimurium models.

Software and tools. Construction and analysis of the model was carried out using the ScrumPy software package (Poolman, 2006) (http://mudshark.brookes.ac.uk/ScrumPy). The package contains a set of modelling tools including those with the ability to interrogate BioCyc databases, perform LP calculations (using GLPK; http://www.gnu.org/software/glpk/) and generate dendrograms (using the ETE toolkit; Huerta-Cepas *et al.*, 2010).

Determination of macromolecular composition of *S.* Typhimurium biomass. In order to determine the macromolecular biomass composition, *S.* Typhimurium LT2 cells were grown in minimal mineral salts medium: M9 medium with 0.5 g glucose l^{-1} as the sole carbon source. Dry cell weight was measured after lyophilization for 16–20 h in triplicate (biological and technical repeats) on a Sartorius balance sensitive up to the fifth decimal. An aliquot of 5 ml of culture was centrifuged for 10 min at 5000 *g*, washed three times in PBS and resuspended in 1 ml of sterile molecular-biology-grade water before lyophilization. Total molecular component content analysis was done using Quant-IT technology (Invitrogen), wherein proprietary fluorophores bind to either the DNA, RNA or protein molecules and the fluorescent intensity corresponds directly to the amount of the target. All fluorescent measurements were performed on a Beckman DTX 8800 plate reader. Amino acid measurements were made on 30 mg lyophilized *Salmonella* cells grown in M9 medium using a Hitachi L8800 Amino Acid Analyser at the University of Texas Medical Branch Biomolecular Resource Centre (Galveston, TX, USA). Carbohydrate analysis was performed (after hydrolysis for 4 h with 20 % TFA) on the lyophilized cell sample using a DX-500 modular ion chromatography system with a CarboPac PA10 analytical column, also at the University of Texas

Medical Branch. Lipids and phospholipids were analysed using 30 mg lyophilized cells using established chromatographic methods at Lipid Analytical Laboratories, University of Guelph Research Park (ON, Canada). All measurements were eventually converted and reported as millimoles of the macromolecular component per gram dry weight of *S.* Typhimurium cells (mmol gDW^{-1}).

***In vivo* validation of predicted cut sets**

Bacterial strains and growth conditions. *S.* Typhimurium ST4/74 was used as the WT strain for experimental validation of model predictions. This strain has been described previously and its virulence is well defined (Wallis *et al.*, 1995). *S.* Typhimurium strains were maintained in LB media (Oxoid). For solid medium, 1.5 % agar was added to give LB agar plates. Chloramphenicol (10 µg ml^{-1}), kanamycin (50 µg ml^{-1}) or carbenicillin (75 µg ml^{-1}) was added as required. Growth phenotypes were investigated in LB (Difco) and M9 minimal media (2 mM MgSO$_4$, 0.1 mM CaCl$_2$, 0.4 % glucose, 8.5 mM NaCl, 42 mM Na$_2$HPO$_4$, 22 mM KH$_2$PO$_4$, 18.6 mM NH$_4$Cl).

Construction of mutant strains. Gene deletions and concomitant insertions of an antibiotic resistance cassette were constructed using Lambda Red-mediated recombination as described elsewhere (Datsenko & Wanner, 2000). All constructs were verified by PCR and moved into a clean background via P22 phage transduction as described previously (Jelsbak *et al.*, 2012). Double- and triple-gene mutants were also constructed by P22-mediated transductions. Primers used to construct mutants are listed in Table S3. At the end, all constructs were verified by restriction analysis and sequencing. Gene numbers refer to the sequenced genome of strain ST4/74 (NCBI-refseq: NC_016857.1) (Richardson *et al.*, 2011).

RESULTS AND DISCUSSION

Biomass composition of *S.* Typhimurium

In the current study, we performed a chemical analysis of the biomass composition of *Salmonella* in terms of amino acids and nucleotides, and compared that with the previous estimates based on *E. coli* (Feist *et al.*, 2007). Overall results are presented in Table 2 (and in detail in Table S1). The composition of *S.* Typhimurium and *E. coli* displayed a relatively high degree of similarity. For the majority of the identified compounds (24 out of 28), the relative difference between the two measurements was <50 %. Greater differences were found for aspartate (65 %), cysteine (68 %), glutamate (63 %) and ATP (76 %). These compounds (except cysteine) had a higher concentration in *Salmonella*.

Consistency and comparison of models

The consistency checks described in Methods were applied to all four models and the results are presented in Table 3. It was further ascertained that the model was able to produce all biomass components (see Table S1) individually and in combination in the experimentally observed proportions.

General model properties

In order to identify and analyse the catabolic core in *S.* Typhimurium, a GSM was constructed. The final model

Table 1. Ten cut sets that influenced ATP generation significantly in damage analysis of the catabolic core of S. Typhimurium and experimental validation of selected pairs

The cut set number refers to the number in Table S7. Reaction abbreviations are consistent with Table S5. The damage is defined as the predicted relative decrease in carbon yield compared with the WT. The mutant phenotype was determined in M9 medium. Detailed growth phenotypes of the mutant strains can be found in Fig. S1.

Cut set	Reaction(s)	Damage (%)	Mutants	Phenotype
1	SucDH	100	$\Delta sdhC$ (STM474-0755)	WT
			$\Delta sdhD$ (STM474-0756)	
			$\Delta sdhC/sdhD$	WT
2	AconDehydr	100	$\Delta acnB$ (STM474-0167)	WT
			$\Delta acnA$ (STM474-1727)	WT
			$\Delta acnA/acnB$	–
3	AconHydr	100	$\Delta acnB$ (STM474-0167)	WT
			$\Delta acnA$ (STM474-1727)	
			$\Delta acnA/acnB$	–
4	GluDH, MalDH	100	$\Delta gdhA$ (STM474-1303)	WT
			Δmdh (STM474-3519)	(WT)
			$\Delta STM3228$	WT
			$\Delta gdh/mdh$	(WT)
			$\Delta mdh/STM3228$	(WT)
			$\Delta gdh/mdh + STM3228$	–
5	Aspartase, MalDH	100	$\Delta aspA$ (STM474-4523)	WT
			$\Delta aspA, mdh$	–
			$\Delta aspA, mdh + STM474-3228$	–
6	THX, MalDH	100	$\Delta pntA$ (STM474-1486)	WT
			$\Delta pntA, mdh$	(WT)
			$\Delta pntA, mdh, STM474-3228$	(–)
7	PGIsomerase, PGLactonase	100	Δpgi (STM474-4415)	(WT)
			$\Delta ybhE$ (STM474-0810)	WT
			$\Delta pji/ybhE$	(WT)
10	MalDH,	100	$\Delta yfbQ$ (STM4747-2428)	WT
	AspTrans		$\Delta yfbQ, mdh$	–
			$\Delta yfbQ, mdh, STM474-3228$	–
16	PGKin	100	pgK (STM474-3216), construction of mutant not possible	ND
17	GapDH	7	gapA (STM474-1294), construction of mutant not possible	ND

(available in ScrumPy and SBML formats in the supplementary model files) has 1097 reactions (ultimately encoded by 824 genes) and 1088 metabolites. See Table 3.

The algorithm of Gevorgyan et al. (2008) was applied to ensure that none of the reactions in the model caused a violation of the law of conservation of mass, essentially as with the models described previously (Poolman et al., 2009, 2013). This ensured complete conservation of C, N, P and S over the whole network. We assumed water to be present in excess and no conservation of water, H_2O_2, OH^- or H^+ (except in the context of the electron transport chain as described above) was enforced. This validation was also applied to the previously published models of S. Typhimurium (AbuOun et al., 2009; Raghunathan et al., 2009; Thiele et al., 2011).

As mentioned, three models of S. Typhimurium metabolism have been constructed (AbuOun et al., 2009; Raghunathan et al., 2009; Thiele et al., 2011). However, the first two [iRR1083 (Raghunathan et al., 2009) and iMA945 (AbuOun et al., 2009)] were constructed by modifying a pre-existing E. coli model [iAF1260 (Feist et al., 2007)], i.e. genetic differences, in terms of presence or absence of genes encoding metabolic enzymes, between E. coli and S. Typhimurium were identified and the relevant reactions subsequently removed from or added to the S. Typhimurium model. A potential problem with this approach is that it might underestimate phenotypic differences between E. coli and S. Typhimurium as genes are analysed in isolation. This is different from the approach used for the construction of organism-specific BioCyc databases, where the set of predicted enzymic reactions of the organism, based on genome sequence alone, is compared with a library of 'canonical' pathways, so that if a critical number of reactions in a given pathway is identified in the set of organism-specific reactions, then all other reactions in that pathway are assumed to be present (Karp et al., 2002). The advantage of this approach is that reactions that are spontaneous or for which there is limited

Table 2. Comparison of concentrations of protein and nucleotide components as measured in *S.* Typhimurium and *E. coli*

Biomass component	Concentration (mmol gDW^{-1})	
	S. Typhimurium	*E. coli*
Amino acids		
Alanine	0.683	0.514
Arginine	0.337	0.296
Asparagine	0.273	0.241
Aspartate	0.682	0.241
Cysteine	0.029	0.092
Glutamate	0.720	0.263
Glutamine	0.20	0.263
Glycine	0.65	0.613
Histidine	0.120	0.095
Isoleucine	0.319	0.291
Leucine	0.527	0.451
Lysine	0.387	0.343
Methionine	0.158	0.154
Phenylalanine	0.216	0.176
Proline	0.240	0.221
Serine	0.308	0.216
Threonine	0.325	0.254
Tryptophan	0.088	0.057
Tyrosine	0.182	0.138
Valine	0.504	0.423
Nucleotides		
ATP	0.108	0.026
CTP	0.120	0.134
GTP	0.134	0.215
UTP	0.111	0.144
dATP	0.031	0.026
dCTP	0.033	0.027
dGTP	0.033	0.027
dTTP	0.031	0.026

enzymic information will still be included. A disadvantage is the potential to overestimate the metabolic capability of the organism.

In contrast to iRR1083 and iMA945, the *S.* Typhimurium consensus model, which is based on iRR1083 and a previously unpublished *S.* Typhimurium model [constructed using the same methodology as that used for iRR1083 (Thiele *et al.*, 2011)], contained 427 unconserved metabolites. So, although more detailed and larger than the previous models, this model suffers from the drawback that approximately a fifth of the metabolites are inconsistent. A consequence of these inconsistencies is the potential for flux distributions that violates the law of mass conservation, i.e. the appearance (or disappearance) of material from nothing. For these reasons, the model presented here was constructed *de novo* from the *S.* Typhimurium genome and thoroughly curated to ensure stoichiometric consistency.

The solution to equation 1 showed that 248 reactions (excluding artificial transporters) were required for growth and maintenance (these reactions are collected in Table S6), corresponding to 268 identifiable genes, which covers 98 % of the reactions in the solution.

Model analysis

In the current study, we propose a new strategy for identifying antimicrobial drug targets based upon the assumption that the ability to regenerate ATP is crucial for the virulence of a pathogen and thus that interference with this process will reduce virulence. In order to evaluate this strategy, we applied a three-step procedure. (i) We identified a set of reactions that responded to changes in demand for ATP. This subset of reactions was denoted the catabolic core. (ii) The catabolic core was subjected to more exhaustive analysis in order to identify those sets of reactions whose joint inhibition abolished its ability to regenerate ATP (cut sets). (iii) The effect of inhibiting these reactions in the whole model on its ability to synthesize biomass precursors was assessed.

Modelling and most experimental analyses were carried out with glucose as the sole carbon source, as our motivation for this initial work was to investigate the potential to identify reactions involved in ATP synthesis as putative drug targets.

Table 3. Properties of various *S.* Typhimurium models

MetaSal is the model presented in this study, iRR1083 was the first published *S.* Typhimurium model, iMA945 was the second published *S.* Typhimurium model and MR is the consensus model. The number of exchange reactions was normalized for the four models so that only minimal glucose medium was available and they were capable of producing the same metabolic byproducts. Values for reactions and metabolites include transporters and boundary metabolites respectively.

Model	Reactions	Dead reactions	Inconsistent subsets	Energy consistency	Metabolites	Unconserved metabolites
MetaSal	1097	497	13	Yes	1088	10
iRR1083	1103	460	20	Yes	959	0
iMA945	1991	946	64	Yes	1740	0
MR	2208	945	45	No	1811	427

Although *S.* Typhimurium is capable of utilizing a number of different substrates during its encounter with the host (including carbohydrates) (Steeb *et al.*, 2013), it exhibits, as do most heterotrophic bacteria, carbon catabolite repression (Görke & Stülke, 2008) (i.e. it shows a strong preference for glucose over other carbon sources). Moreover, alternative carbon sources that are available during intracellular infection, primarily hexose phosphates, would be catabolized by a subset of reactions involved with glucose catabolism. Thus, by analysing with glucose as the source, we have created a conservative estimate of targets, i.e. eliminating reactions concerned with the catabolism of other carbon sources would potentially only be relevant for that source, whilst any block of glucose catabolism would also interfere with the catabolism of other possible sources.

Catabolic core and its properties

Of the 306 reactions that were found to be required for synthesis of biomass, 33 responded to the variation in ATP demand and we defined these as the catabolic core. These fluxes could be grouped into six sets of correlated responses (Fig. 1).

The isolated catabolic core forms a single connected network (Fig. 2), comprising mainly the reactions of glycolysis, the TCA cycle and the Entner–Doudoroff pathway. Flux through the catabolic core (Fig. 3) involves exchange of metabolites with the main network, mostly at a rate unaffected by the ATP demand (Table 4). This is due to the constraints that the solutions to the LP defined must produce biomass precursors and regenerate ATP. The catabolic core has a total of six subsets, which allow it to be redrawn in condensed form (Fig. 4); the net stoichiometries of these subsets are summarized in Table 5.

MCSs of the catabolic core

The concept of a MCS, in the context of metabolic network analysis, was introduced by Klamt & Gilles (2004) and defined as a minimal set of reactions whose removal will result in the abolition of steady-state flux in a target reaction. In the current study, we applied this idea to identify sets of reactions whose joint inhibition leads to the abolition of ATP production.

The condensed catabolic core was found to contain six MCSs (Table 3): two composed of a single cut and four of a double cut. In terms of the uncondensed catabolic core, any of the reactions of subsets 2 and 5 are MCSs of size 1. MCSs of size 2 can be formed by combining pairs of reactions from subsets 1 and 3, 1 and THX, 3 and THX or 4 and 6. Hence, the six MCSs of the condensed model expand to a total of 49 MCSs in the uncondensed catabolic core (see Table S7).

Although these 49 MCSs abolished ATP production in the isolated catabolic core, it remained possible that they could
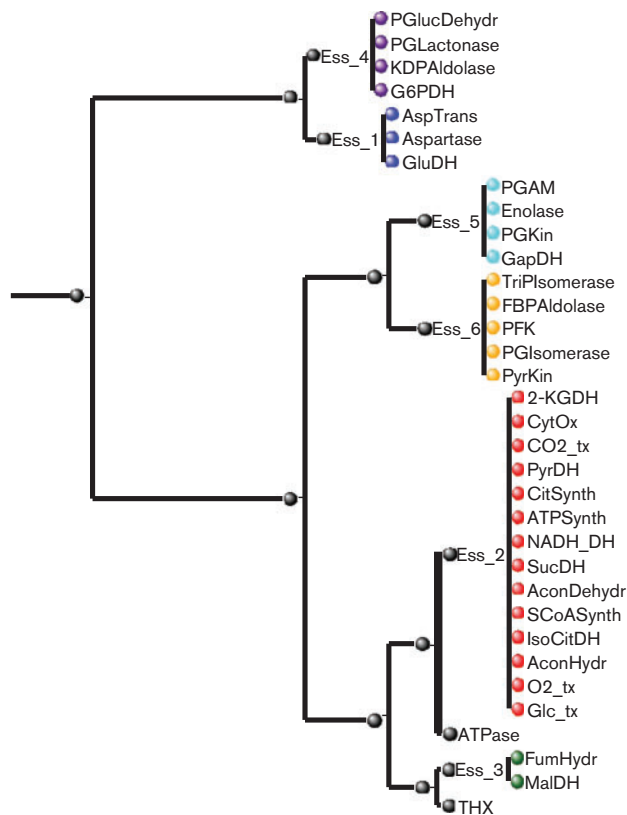

Fig. 1. Flux correlation tree of the reactions of the catabolic core network. The tree shows correlations in flux response to the imposed ATP demand between reactions in the catabolic core model. Enzyme subset identities of the reactions are indicated by colour codes, corresponding to those used in Fig. 4. See Table S5 in the online Supplementary Material for abbreviations and BioCyc identifiers of reactions and metabolites.

be bypassed by reactions outside the catabolic core but present in the full metabolic network. Evaluation of the impact of these proposed MCSs on the whole model was therefore performed. This revealed that 11 MCSs were lethal, i.e. no solution to equation 1 existed, whilst for 38 MCSs a solution existed, but with a higher objective value, i.e. the network needed to invest more total flux to satisfy the constraints. The damage imposed by the MCSs expressed as change (from WT) in biomass yield and objective value are shown in Fig. 5 (and in more detail in Table S7).

By repeating the catabolic core extraction (note that owing to the energy inconsistency in the consensus model, catabolic core extraction could only be performed after forcing a magnesium transporter to carry zero flux) and MCS analysis on the three other *S.* Typhimurium models, some conserved cut sets could be identified. The two aconitase reactions were both lethal in all models, except iRR1083. Phosphoglycerate kinase appeared in all models with intermediate damage: the increase in objective value
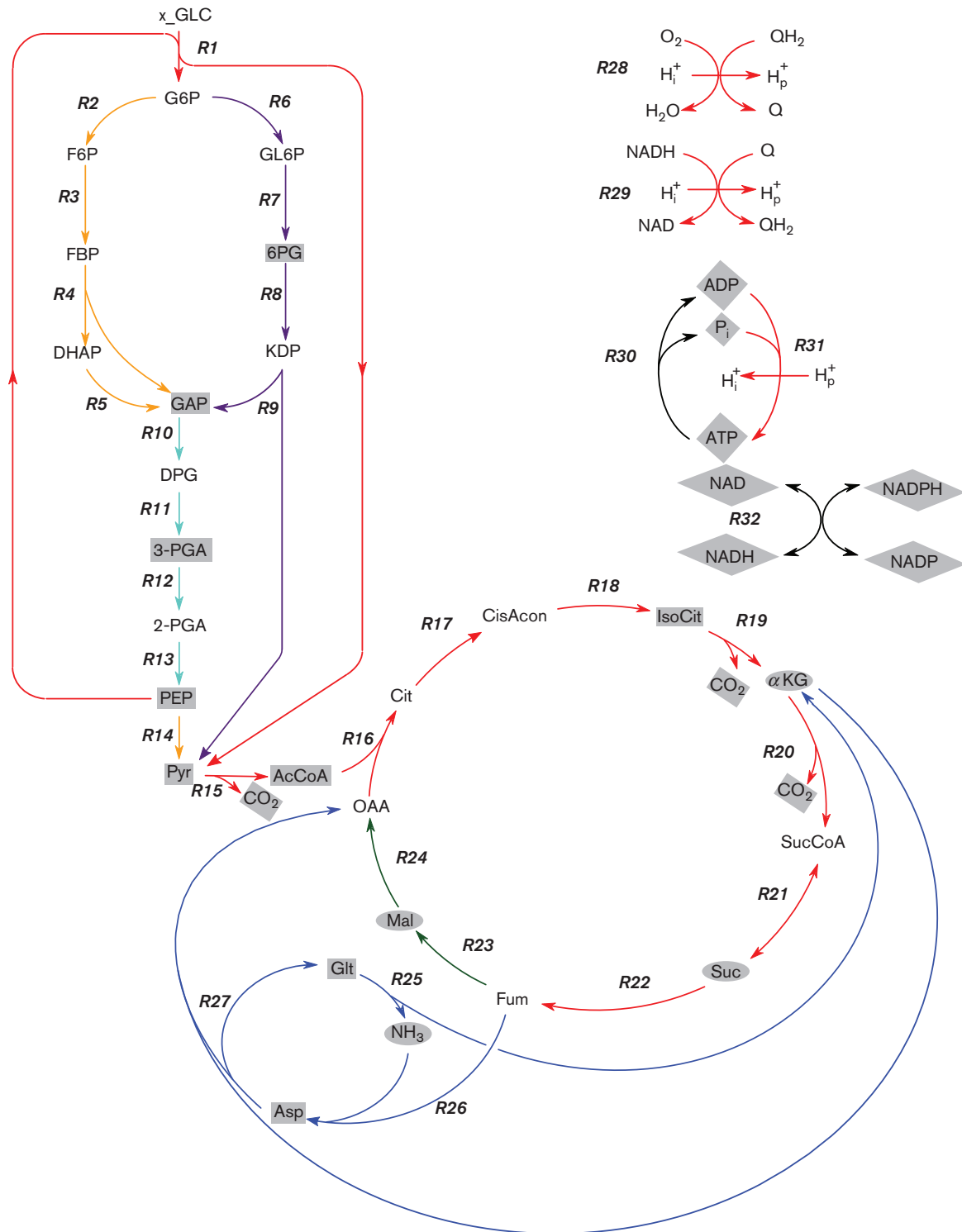
Fig. 2. The catabolic core. Reactions are coloured according to the groupings identified in Fig. 1. Metabolites with grey backgrounds are imported (ovals) or exported (rectangles) from and to the remainder of the network at a fixed rate. Metabolites whose transport can be decomposed into a variable and fixed component are indicated with diamond-shaped backgrounds. Abbreviations are consistent with Table S5. See also Table 4. Key: R1, Glc transport; R2, PGI; R3, PFK; R4, FBPAldolase; R5, TPI; R6, G6PDH; R7, PGLactonase; R8, PGlucDH; R9, KDPAldolase; R10, GapDH; R11, PGK; R12, PGAM; R13, enolase; R14, PyrKin; R15, PyrDH; R16, CitSynth; R17, AconDehydr; R18, AconHydr; R19, IsoCitDH; R20, 2-KGDH; R21, SucCoASynth; R22, SucDH; R23, FumHyd; R24, MalDH; R25, GluDH; R26, aspartase; R27, AspTrans; R28, CytOx; R29, NADH DH; R30, ATPase; R31, ATPSynth; R32, THX.
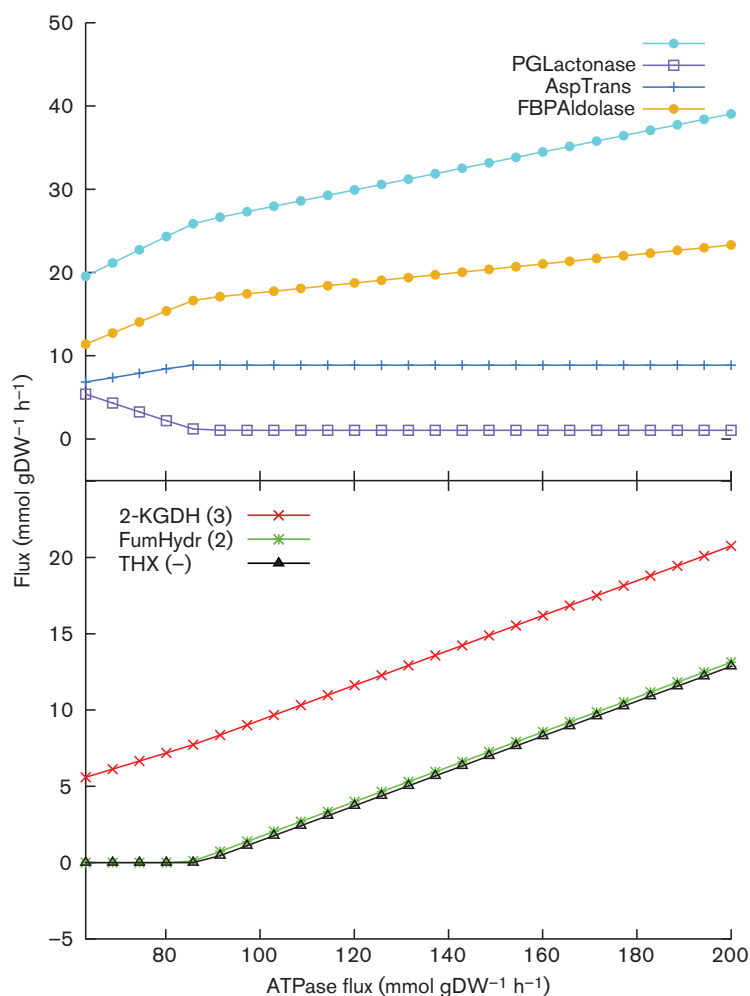
Fig. 3. Flux response of the GSM to ATP demand variation. Only responses of reactions that displayed non-constant flux, i.e. the reactions of the catalytic core, are displayed. Each reaction is a representative of an enzyme subset (indicated in brackets). The colours of the response curves are in accordance with those of Fig. 2. Abbreviations are consistent with Table S5.

ranged from 27 (in the consensus model) and 29 % (in iMA945) to 40 (iRR1083) and 52 % (in the model presented here). The damage caused by removing glyceraldehyde 3-phosphate dehydrogenase was identical to the damage caused by removing phosphoglycerate kinase, which is to be expected as they appear in the same subset. Removal of enolase caused similar damage in the model presented here (33 % increase in objective value), iMA945 (21 % increase), iRR1083 (17 % increase) and the consensus model (14 % increase). Another example is phosphoglycerate mutase, which when removed from the models caused similar damage: 17 % increase in iRR1083, 21 % increase in iMA945, 14 % increase in the consensus model and 33 % increase in the model presented here. (Detailed results are presented in Tables S8–S10.)

Examining the catabolic core for aerobic glucose-based metabolism in its condensed form allowed for a clearer view as to how the 34 reactions acted as an integrated whole, something also revealed by the correlation of fluxes identified from equation 2. Most, but not all, of the reactions in the catabolic core corresponded to familiar pathways generally assumed to be involved with energy metabolism. No previous model work detailing the

catabolic core of bacteria is available. The catabolic core determined in *S.* Typhimurium has many points of similarity, and some specific differences, to that obtained from the model of *Arabidopsis thaliana* using the same modelling methodology (Poolman *et al.*, 2009): they both utilize glycolysis, the TCA cycle and the oxidative component of the oxidative pentose phosphate pathway in a comparable fashion.

In contrast to *A. thaliana*, the catabolic core described here did not include the rest of the pentose pathway nor, obviously, the photosynthetic reactions observed in *A. thaliana*. There is, however, a functional relationship between subset 1 and the photosynthetic reactions in that they both act to bypass parts of the TCA cycle by involving reactions associated with NH_3 assimilation.

Experimental and theoretical validation of MCSs

The cut set analysis suggested that the simultaneous inhibition of two reactions is likely to be much more deleterious to the organism than inhibiting a single reaction. Of the 49 cut sets identified (i.e. sets of reactions that when removed from the catabolic core abolished ATP

Table 4. Major metabolite exchange between the catabolic core and the rest of the network (flux below 1.00 mmol gDW^{-1} h^{-1} has been omitted)

'Reactions' refers to the number of reactions outside the catabolic core utilizing the corresponding metabolite. Note that the total flux involving P_i, ATP and ADP can be split into a variable component (which is a response to the imposed ATPase flux) and a constant component (which is a response to the constant energy demand from the anabolic reactions). Also, the flux of CO_2 can be split into a constant import rate and the variable export of CO_2 to the external medium. Abbreviations are consistent with Table S5.

Metabolite	Import flux	Reactions	Metabolite	Export flux		Reactions
$P_{i,constant}$	37	36	$ATP_{constant}$	63.0	24.6	45
$P_{i,variable}$	63.0–200.0	–	$ATP_{variable}$		−200	–
$ADP_{constant}$	26.4	30	$CO_{2variable}$	35.0	−81.0	–
$ADP_{variable}$	63.0–200.0	–	NADPH		12.5	25
NH_3	12.56	12	GLT		9.8	21
NADP	12.5	26	Pyr		9.7	10
NADH	8.7	12	NAD		8.7	14
αKG	8.6	10	AcCoA		6.0	6
$CO_{2constant}$	8.5	10	GAP		5.0	5
CoA	6.8	8	IsoCit		2.8	1
Suc	4.6	4	3-PGA		2.0	1
Mal	3.8	1	Asp		2.8	9
			PEP		1.4	5
			6PG		1.1	1

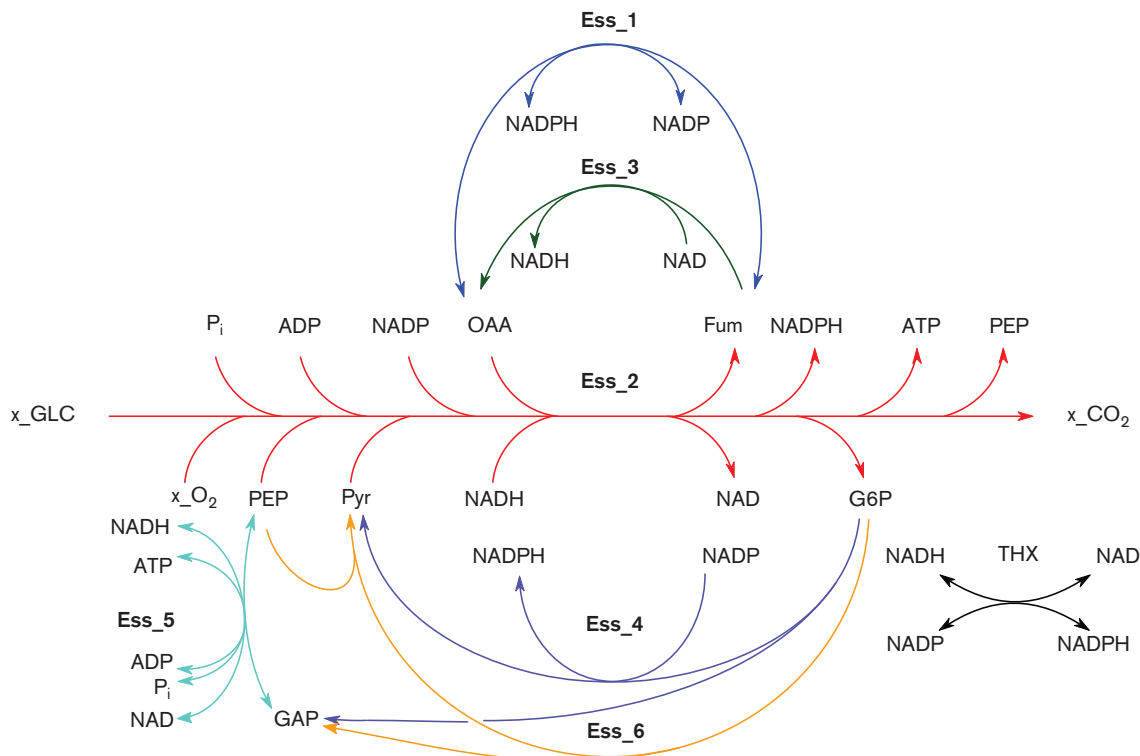**Fig. 4.** The condensed catabolic core. The colour of each subset corresponds to those of their component reactions as shown in Figs 1 and 2. The cut sets that abolished ATP generation were: Ess_2, Ess_5, Ess_1 and Ess_3, Ess_1 and THX, Ess_3 and THX, and Ess_4 and Ess_6 (i.e. Ess_2 and Ess_5 were essential sets, the other sets were reaction pairs). Abbreviations are consistent with Table S5.

Table 5. Stoichiometry of enzyme subsets generated from the catabolic core model

The condensed net stoichiometry is shown for each enzyme subset of the core network. The reversibility of each subset is indicated by the reaction stoichiometry of the condensed reaction. External metabolites are indicated by the prefix 'x_' and abbreviations are consistent with Table S5.

Enzyme subset	Stoichiometry		
	Reactants		Products
Ess_1	$Fum + NADP$	$\leftrightarrow$	$NADPH + OAA$
Ess_2	$PEP + 17P_i + 6x\_O_2 + 6NADH + 17ADP + 2NADP + x\_Glc + Pyr + 2OAA$	$\rightarrow$	$6x\_CO_2 + 6NAD + 2Fum + 2NADPH + 17ATP + G6P$
Ess_3	$NADH + OAA$	$\leftrightarrow$	$Fum + NAD$
Ess_4	$NADP + G6P$	$\rightarrow$	$NADPH + Pyr + GAP$
Ess_5	$NAD + GAP + ADP + P_i$	$\leftrightarrow$	$NADH + ATP + PEP$
Ess_6	$PEP + G6P$	$\rightarrow$	$Pyr + 2GAP$
THX	$NAD + NADPH$	$\leftrightarrow$	$NADH + NADP$

production), 11 were lethal (i.e. no solution to equation 1 existed) and five resulted in intermediate damage (decreased the carbon yield by ~50 % or significant increase in sum of fluxes). On the basis of this, we were able to propose 16 cut sets for experimental work, out of which seven were constructed and validated (Table 1 and in more detail in Fig. S1). Single and, where needed, double mutants were constructed in *S*. Typhimurium ST4/74, a derivative of strain SL1344. Small differences exist between the annotated genomes of this strain and of strain LT2, and we cannot rule out that this has affected results.

All cut sets were associated with two genes. Three of the sets were singletons (succinate dehydrogenase and the two aconitase reactions) and the remaining four sets were pairs (glutamate dehydrogenase and malate dehydrogenase; aspartase and malate dehydrogenase; transhydrogenase and malate dehydrogenase; 6-phosphogluconolactonase and glucose 6-phosphate isomerase). Succinate dehydrogenase has been shown to be essential for growth in LB in *E. coli* (Yu *et al.*, 2006) and so the essentiality in *S.* Typhimurium is not surprising. The genes *acnAB*, mapping to the two singleton aconitase cut sets, have been shown to be an essential pair in *E. coli* (Gruer *et al.*, 1997) and more recently (Baothman *et al.*, 2013) in *S*. Typhimurium. To the best of our knowledge, this is the first reported experimental validation of the essentiality of the four reaction pairs in *S*. Typhimurium. However, as described in more detail below, Δ*mdh* strains have been shown to be attenuated *in vivo*.

Interestingly, seven of the lethal cut sets involved reactions associated with amino acid biosynthesis/degradation (subset 1) and the Entner–Doudoroff pathway (subset 4), and all of the cut sets with intermediate damage included the Entner–Doudoroff reactions, strengthening the proposal that these reactions have a significant role in energy metabolism. This finding is supported by previous experimental observations (Cohen, 2010).

Some of the TCA cycle reactions identified as members of cut sets in this study have also been subject to deletion

studies in *S*. Typhimurium. Tchawa Yimga *et al.* (2006) investigated the effect on virulence of disrupting various parts of the TCA cycle in *S*. Typhimurium. It was concluded that a functional TCA cycle was required for successful infection based upon the observations that deletion of *sucAB* (encoding 2-oxoglutarate dehydrogenase) resulted in avirulence, deletion of *mdh* (encoding malate dehydrogenase) resulted in strong attenuation and deletion of *sucCD* (encoding succinate-CoA synthase) resulted in moderate attenuation. In a subsequent study, the double mutation Δ*sdhCDA*, Δ*frdABCD* (deletion of the isoenzymes fumarate reductase and succinate dehydrogenase) resulted in an avirulent strain (Mercado-Lubo *et al.*, 2008).

For validation, we set out to compare growth in LB and M9 minimal media of the WT (which grew in both media, data not shown) with single, double and triple mutants of 10 cut sets (Table 1). Construction of mutants in *gapA* (STM474-1294) and *pkk* (STM474-3216) was, however, not possible despite several attempts, suggesting that these genes were essential for growth of *S*. Typhimurium under the conditions used to construct mutants. *gapA* is associated with glyceraldehyde 3-phosphate dehydrogenase which is central in the glycolysis. This pathway is essential for survival of *S*. Typhimurium in mice and macrophages (Bowden *et al.*, 2009). Attempts have not previously been reported to delete this particular gene, but the fact that this gene did not come up as a mutated gene in the genome-wide screen for the effects of gene knockouts reported by Chaudhuri *et al.* (2009) supports our observation.

Phosphoglycerate kinase is associated with *pkk* and is also an essential part of glycolysis; this gene too was not hit by transposons in the mutants harvested by Chaudhuri *et al.* (2009). In addition to being involved in glycolysis, the two reactions are also essential for glyconeogenesis. Both of these reactions were identified by Becker *et al.* (2006) as essential during infection. For the remaining eight reactions, we investigated 12 single, eight double and four triple mutants of strain ST4/74 (Table 1). All mutants grew similarly to the WT strain in LB media (Table 1),
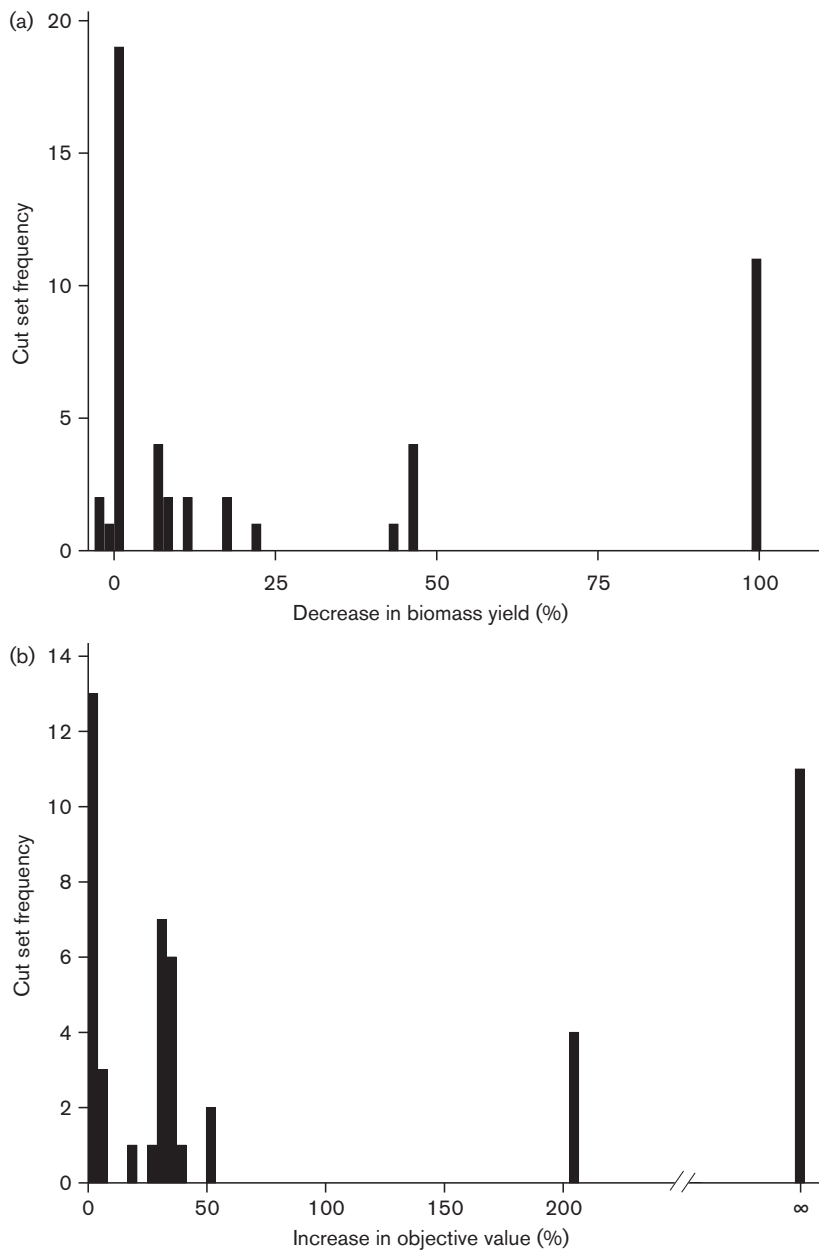
Fig. 5. Distribution of damage, expressed as (a) percentage decrease in biomass yield on glucose and (b) percentage increase in objective value caused by constraining fluxes in reactions of the MCSs of the catabolic core to the whole model. This is assumed to be (a) 100 % and (b) infinity for the 11 MCSs that resulted in equation 4 becoming infeasible. The WT objective value and biomass yield were 445 mmol gDW^{-1} h^{-1} and 0.81, respectively. Abbreviations are consistent with Table S5.

suggesting that in rich media *S*. Typhimurium can compensate for the loss of all these reactions through uptake of nutrients from the media. *Salmonella* can use a diversity of carbon sources *in vivo* (Steeb *et al.*, 2013). LB and M9 media do not resemble the nutritional conditions *in vivo*, and infection studies are required before our cut sets can be judged with respect to new targets for antibiotics. Also, since the catabolic core resembles the eukaryotic core (Poolman *et al.*, 2009), it is unknown whether prokaryotic specific inhibitors are available.

Single or simultaneous removal of the reactions cut set 7 (glucose 6-phosphate isomerase and 6-phosphogluconolactonase) was shown not to be lethal for growth in M9 medium, but to cause a slight growth attenuation (Table 1),

which indicates that the first part of the glycolysis (glucose 6-phosphate isomerase) and the pentose phosphate pathway (6-phosphogluconolactonase) are not absolutely essential for growth, but that growth is less efficient when they are both blocked. Bowden *et al.* (2009) used the redundant pair *pfkA*, *pfkB* to investigate the importance of glycolysis, and succeeded in isolating both single and double mutants. These genes encode the enzymes responsible for the initial conversion of D-fructose 6-phosphate, which is only part of glycolysis and not of gluconeogenesis. As they succeeded in constructing a viable double mutant and we demonstrated that *pgi* (STM474-4415) encoding the enzyme for glucose 6-phosphate isomerase was not essential for growth (and is not essential for infection; Chaudhuri *et al.*, 2009), this indicates

that glycolysis and gluconeogenesis must be blocked at the same time in S. Typhimurium before growth is inhibited.

The two aconitase reactions (sets 2 and 3 in Table 1) in the TCA cycle were both associated with the same two genes, *acnA* (STM4747-1727) and *acnB* (STM474-0167). Blocking the TCA cycle at both places was shown to abolish the ability to grow in minimal medium (Table 1). AcnB has been reported to be the major Acn protein in S. Typhimurium; however, unlike *E. coli*, *acnA* appears to be upregulated in the absence of *acnB* and can thus compensate for this enzyme (Baothman *et al.*, 2013). In confirmation of this, we saw no difference in growth capacity between the two single-enzyme mutants. The TCA cycle is not important during S. Typhimurium interaction with cultured macrophages as cells with a deleted TCA cycle show higher intracellular replication than the WT strain (Bowden *et al.*, 2010); however, *acnB* mutation caused a significantly reduced fitness during mouse infection (Chaudhuri *et al.*, 2009). This investigation constitutes the first report that combined deletion of *acnA* and *acnB* renders S. Typhimurium unable to grow in minimal medium. Several other cut sets included enzymes of the TCA cycle, demonstrating the central role of this cycle in energy production.

The model predicted that cut set 1 (succinate dehydrogenase) would be essential for energy production. However, as the only cut set investigated, double mutation of the involved enzymes (*sdhC* and *sdhD*; STM4747-0755 and STM4747-0756) did not cause any phenotype (Table 1). The reaction is annotated differently in strain LT2 (model strain) and ST4/74 (validation strain), and this may represent a mistake in annotation in one of the strains. However, the genes are in an operon, and elimination of *sdhC* and *sdhD* should abolish expression of *sdhA* and *sdhB* as well. Mercado-Lubo *et al.* (2008) constructed an *sdhA*, *sdhB*, *sdhC* triple mutant, and showed that this strain was slightly attenuated during mice infection. However, they did not investigate the growth phenotype on minimal medium.

An *mdh* mutant was also attenuated in that study, and the combined deletion of succinate dehydrogenase and malate dehydrogenase was suggested as a good live vaccine candidate (Mercado-Lubo *et al.*, 2008). In the current study, four of the cut sets predicted to be lethal included the malate dehydrogenase reaction (Table 1, reaction sets 4, 5, 6 and 10). In strain ST4/74, this reaction in the TCA cycle is also annotated with *mdh* (STM4747-3519) and a putative malate dehydrogenase encoded from STM474-3228, and we therefore eliminated these two genes together. However, the elimination of STM4747-3228 did not confer a phenotype, whilst *mdh* deletion resulted in a slightly decreased ability to grow in M9 minimal medium (Table 1). When this part of the TCA cycle was deleted together with either glutamate dehydrogenase (cut set 4), which feeds 2-oxoglutarate into the TCA cycle from glutamate, aspartase (cut set 5), which feeds fumarate into the TCA cycle from L-aspartate, the membrane bound transhydrogenase

reaction (set 6), which in *E. coli* is essential for balancing the NADH pool (Fuhrer & Sauer, 2009), or aspartate aminotransferase (cut set 10), which makes L-aspartate from L-glutamate, growth was reduced or totally inhibited, as predicted by the model.

In the case of glutamate dehydrogenase (set 4) and transhydrogenase (set 6), deletion of STM4747-3228 conferred an additional growth inhibition that was not seen with the two primary enzymes, suggesting that this putative enzyme has a role in these particular reactions (Table 1). Together the results indicate that when the formation of fumarate is blocked, growth ceases in S. Typhimurium. Resources did not allow for experimental validation of all predictions.

The five cut sets with only 50 % reduction in ATP yield were left out, since the growth phenotypes were anticipated to be indistinguishable from WT. Cut set 13 (fructose bisphosphate aldolase and phosphogluconate dehydratase, in glycolysis and the Entner–Doudoroff pathway, respectively) was also not easy to analyse, as fructose bisphosphate aldolase is annotated with seven genes in S. Typhimurium ST4/74.

Cut set 15 (2-keto-3-deoxy-6-phosphogluconic aldolase and 6-phosphofructokinase, also in the Entner–Doudoroff pathway and glycolysis, respectively) has been partly investigate by Bowden *et al.* (2009) who produced a combined knockout of *pfkA*, *pfkB*. The gene *eda* (STM474-1916) encoding the enzyme 2-keto-3-deoxy-6-phosphogluconic aldolase of the Entner–Doudoroff pathway has an orthologue in strain LT2 (*dga*) (Miller *et al.*, 2013), but apparently this is not present in strain ST4/74. *eda* is not essential for mouse virulence (Chaudhuri *et al.*, 2009). Sets 12 (fructose bisphosphate aldolase and 2-keto-3-deoxy-6-phosphogluconic aldolase, in glycolysis and the Entner–Doudoroff pathway, respectively) and 14 (6-phosphofructokinase and phosphogluconate dehydratase in glycolysis and the Entner–Doudoroff pathway, respectively) were combinations of reactions mentioned above, whilst ATP synthesis is encoded by many different genes. The fact that the model indicates that elimination of so many combinations of reactions in glycolysis and the Entner–Doudoroff pathway at the same time only confers 50 % reduction of carbon yield deserves experimental confirmation as it indicates that they can be blocked in parallel without eliminating growth.

The three remaining sets were cut sets 9 (glucose 6-phosphate 1-dehydrogenase and glucose 6-phosphate isomerase, another combination of the pentose phosphate pathway and glycolysis), 8 (aspartase and fumarate hydratase) and 11 (fumarate hydratase and aspartate aminotransferase). The latter two cut sets both block fumarate synthesis and the TCA cycle, which we had already investigated.

In conclusion, we have identified a functional subnetwork of reactions responsible for ATP regeneration which could be isolated from a GSM of S. Typhimurium. By condensing the network to subsets, much of the apparent complexity of

the network was reduced without loss of information and condensation greatly simplified damage analysis. Based on evaluation of the damage imposed on the global model by the cut sets obtained from the condensed network, we have suggested 16 cut sets and demonstrated that seven of these abolished or attenuated growth of the organism in glucose minimal medium.

ACKNOWLEDGEMENTS

REFERENCES

AbuOun, M., Suthers, P. F., Jones, G. I., Carter, B. R., Saunders, M. P., Maranas, C. D., Woodward, M. J. & Anjum, M. F. (2009). Genome scale reconstruction of a *Salmonella* metabolic model: comparison of similarity and differences with a commensal *Escherichia coli* strain. *J Biol Chem* **284**, 29480–29488.

Andries, K., Verhasselt, P., Guillemont, J., Göhlmann, H. W. H., Neefs, J.-M., Winkler, H., Van Gestel, J., Timmerman, P., Zhu, M. & other authors (2005). A diarylquinoline drug active on the ATP synthase of *Mycobacterium tuberculosis. Science* **307**, 223–227.

Baothman, O. A. S., Rolfe, M. D. & Green, J. (2013). Characterization of *Salmonella enterica* serovar Typhimurium aconitase A. *Microbiology* **159**, 1209–1216.

Bauchop, T. & Elsden, S. R. (1960). The growth of micro-organisms in relation to their energy supply. *J Gen Microbiol* **23**, 457–469.

Becker, D., Selbach, M., Rollenhagen, C., Ballmaier, M., Meyer, T. F., Mann, M. & Bumann, D. (2006). Robust *Salmonella* metabolism limits possibilities for new antimicrobials. *Nature* **440**, 303–307.

Bowden, S. D., Rowley, G., Hinton, J. C. D. & Thompson, A. (2009). Glucose and glycolysis are required for the successful infection of macrophages and mice by *Salmonella enterica* serovar Typhimurium. *Infect Immun* **77**, 3117–3126.

Bowden, S. D., Ramachandran, V. K., Knudsen, G. M., Hinton, J. C. & Thompson, A. (2010). An incomplete TCA cycle increases survival of *Salmonella* Typhimurium during infection of resting and activated murine macrophages. *PLoS ONE* **5**, e13871.

Cano, D. A., Pucciarelli, M. G., Martínez-Moya, M., Casadesús, J. & García-del Portillo, F. (2003). Selection of small-colony variants of *Salmonella enterica* serovar Typhimurium in nonphagocytic eucaryotic cells. *Infect Immun* **71**, 3690–3698.

Chaudhuri, R. R., Peters, S. E., Pleasance, S. J., Northen, H., Willers, C., Paterson, G. K., Cone, D. B., Allen, A. G., Owen, P. J. & other authors (2009). Comprehensive identification of *Salmonella enterica* serovar Typhimurium genes required for infection of BALB/c mice. *PLoS Pathog* **5**, e1000529.

Cohen, P. S. (2010). Live attenuated aldose-negative bacterial vaccine. US Patent US 20100003284.A1.

Datsenko, K. A. & Wanner, B. L. (2000). One-step inactivation of chromosomal genes in *Escherichia coli* K-12 using PCR products. *Proc Natl Acad Sci U S A* **97**, 6640–6645.

Edwards, J. S. & Palsson, B. O. (2000). The *Escherichia coli* MG1655 *in silico* metabolic genotype: its definition, characteristics, and capabilities. *Proc Natl Acad Sci U S A* **97**, 5528–5533.

Feist, A. M., Henry, C. S., Reed, J. L., Krummenacker, M., Joyce, A. R., Karp, P. D., Broadbelt, L. J., Hatzimanikatis, V. & Palsson, B. O. (2007). A genome-scale metabolic reconstruction for *Escherichia coli* K-12 MG1655 that accounts for 1260 ORFs and thermodynamic information. *Mol Syst Biol* **3**, 121.

Fell, D. A. & Small, J. R. (1986). Fat synthesis in adipose tissue. An examination of stoichiometric constraints. *Biochem J* **238**, 781–786.

Fuhrer, T. & Sauer, U. (2009). Different biochemical mechanisms ensure network-wide balancing of reducing equivalents in microbial metabolism. *J Bacteriol* **191**, 2112–2121.

García-del Portillo, F., Núñez-Hernández, C., Eisman, B. & Ramos-Vivas, J. (2008). Growth control in the *Salmonella*-containing vacuole. *Curr Opin Microbiol* **11**, 46–52.

Gevorgyan, A., Poolman, M. G. & Fell, D. A. (2008). Detection of stoichiometric inconsistencies in biomolecular models. *Bioinformatics* **24**, 2245–2251.

Görke, B. & Stülke, J. (2008). Carbon catabolite repression in bacteria: many ways to make the most out of nutrients. *Nat Rev Microbiol* **6**, 613–624.

Gruer, M. J., Bradbury, A. J. & Guest, J. R. (1997). Construction and properties of aconitase mutants of *Escherichia coli. Microbiology* **143**, 1837–1846.

Holzhütter, H.-G. (2004). The principle of flux minimization and its application to estimate stationary fluxes in metabolic networks. *Eur J Biochem* **271**, 2905–2922.

Holzhütter, H.-G. (2006). The generalized flux-minimization method and its application to metabolic networks affected by enzyme deficiencies. *Biosystems* **83**, 98–107.

Huerta-Cepas, J., Dopazo, J. & Gabaldón, T. (2010). ETE: a Python environment for tree exploration. *BMC Bioinformatics* **11**, 24.

Hughes, J. A. (2006). *In vivo* hydrolysis of *S*-adenosyl-L-methionine in *Escherichia coli* increases export of 5-methylthioribose. *Can J Microbiol* **52**, 599–602.

Jelsbak, L., Thomsen, L. E., Wallrodt, I., Jensen, P. R. & Olsen, J. E. (2012). Polyamines are required for virulence in *Salmonella enterica* serovar Typhimurium. *PLoS ONE* **7**, e36149.

Karp, P. D., Paley, S. & Romero, P. (2002). The Pathway Tools software. *Bioinformatics* **18** (Suppl. 1), S225–S232.

Klamt, S. & Gilles, E. D. (2004). Minimal cut sets in biochemical reaction networks. *Bioinformatics* **20**, 226–234.

Maloney, P. C. (1987). Coupling to an energized membrane: role of ion-motive gradients in the tranduction of metabolic energy. In *Escherichia Coli and Salmonella Typhimurium. Cellular and Molecular Biology*, vol. 1, pp. 222–243. Edited by F. C. Neidhardt. Washington, DC: American Society for Microbiology.

McClelland, M., Sanderson, K. E., Spieth, J., Clifton, S. W., Latreille, P., Courtney, L., Porwollik, S., Ali, J., Dante, M. & other authors (2001). Complete genome sequence of *Salmonella enterica* serovar Typhimurium LT2. *Nature* **413**, 852–856.

Mercado-Lubo, R., Gauger, E. J., Leatham, M. P., Conway, T. & Cohen, P. S. (2008). A *Salmonella enterica* serovar Typhimurium succinate dehydrogenase/fumarate reductase double mutant is avirulent and immunogenic in BALB/c mice. *Infect Immun* **76**, 1128–1134.

Miller, K. A., Phillips, R. S., Mrázek, J. & Hoover, T. R. (2013). *Salmonella* utilizes D-glucosaminate via a mannose family phosphotransferase system permease and associated enzymes. *J Bacteriol* **195**, 4057–4066.

Murphy, D. J. & Brown, J. R. (2007). Identification of gene targets against dormant phase *Mycobacterium tuberculosis* infections. *BMC Infect Dis* **7**, 84.

Norrby, S. R., Nord, C. E., Finch, R. & European Society of Clinical Microbiology and Infectious Diseases (2005). Lack of development of new antimicrobial drugs: a potential serious threat to public health. *Lancet Infect Dis* **5**, 115–119.

Paterson, D. L. (2006). Resistance in gram-negative bacteria: Enterobacteriaceae. *Am J Med* **119** (Suppl. 1), S20–S28, discussion S62–S70.

Pfeiffer, T., Sánchez-Valdenebro, I., Nuño, J. C., Montero, F. & Schuster, S. (1999). METATOOL: for studying metabolic networks. *Bioinformatics* **15**, 251–257.

Poolman, M. G. (2006). ScrumPy: metabolic modelling with Python. *Syst Biol (Stevenage)* **153** (5), 375–378.

Poolman, M. G., Sebu, C., Pidcock, M. K. & Fell, D. A. (2007). Modular decomposition of metabolic systems via null-space analysis. *J Theor Biol* **249**, 691–705.

Poolman, M. G., Miguet, L., Sweetlove, L. J. & Fell, D. A. (2009). A genome-scale metabolic model of *Arabidopsis* and some of its properties. *Plant Physiol* **151**, 1570–1581.

Poolman, M. G., Kundu, S., Shaw, R. & Fell, D. A. (2013). Responses to light intensity in a genome-scale model of rice metabolism. *Plant Physiol* **162**, 1060–1072.

Prost, L. R., Sanowar, S. & Miller, S. I. (2007). *Salmonella* sensing of anti-microbial mechanisms to promote survival within macrophages. *Immunol Rev* **219**, 55–65.

Raghunathan, A., Reed, J., Shin, S., Palsson, B. & Daefler, S. (2009). Constraint-based analysis of metabolic capacity of *Salmonella typhimurium* during host–pathogen interaction. *BMC Syst Biol* **3**, 38.

Rao, S. P. S., Alonso, S., Rand, L., Dick, T. & Pethe, K. (2008). The protonmotive force is required for maintaining ATP homeostasis and viability of hypoxic, nonreplicating *Mycobacterium tuberculosis*. *Proc Natl Acad Sci U S A* **105**, 11945–11950.

Richardson, E. J., Limaye, B., Inamdar, H., Datta, A., Manjari, K. S., Pullinger, G. D., Thomson, N. R., Joshi, R. R., Watson, M. & Stevens, M. P. (2011). Genome sequences of *Salmonella enterica* serovar Typhimurium, Choleraesuis, Dublin, and Gallinarum strains of well-defined virulence in food-producing animals. *J Bacteriol* **193**, 3162–3163.

Steeb, B., Claudi, B., Burton, N. A., Tienz, P., Schmidt, A., Farhan, H., Mazé, A. & Bumann, D. (2013). Parallel exploitation of diverse host nutrients enhances *Salmonella* virulence. *PLoS Pathog* **9**, e1003301.

Tchawa Yimga, M., Leatham, M. P., Allen, J. H., Laux, D. C., Conway, T. & Cohen, P. S. (2006). Role of gluconeogenesis and the tricarboxylic acid cycle in the virulence of *Salmonella enterica* serovar Typhimurium in BALB/c mice. *Infect Immun* **74**, 1130–1140.

Thiele, I., Hyduke, D. R., Steeb, B., Fankam, G., Allen, D. K., Bazzani, S., Charusanti, P., Chen, F. C., Fleming, R. M. & other authors (2011). A community effort towards a knowledge-base and mathematical model of the human pathogen *Salmonella* Typhimurium LT2. *BMC Syst Biol* **5**, 8.

Tierrez, A. & García-del Portillo, F. (2005). New concepts in *Salmonella* virulence: the importance of reducing the intracellular growth rate in the host. *Cell Microbiol* **7**, 901–909.

Varma, A. & Palsson, B. O. (1993a). Metabolic capabilities of *Escherichia coli*: I. Synthesis of biosynthetic precursors and cofactors. *J Theor Biol* **165**, 477–502.

Varma, A. & Palsson, B. O. (1993b). Metabolic capabilities of *Escherichia coli*: II. Optimal growth patterns. *J Theor Biol* **165**, 503–522.

Wallis, T. S., Paulin, S. M., Plested, J. S., Watson, P. R. & Jones, P. W. (1995). The Salmonella dublin virulence plasmid mediates systemic but not enteric phases of salmonellosis in cattle. *Infect Immun* **63**, 2755–2761.

Watson, M. R. (1986). A discrete model of bacterial metabolism. *Comput Appl Biosci* **2**, 23–27.

Wayne, L. G. & Sohaskey, C. D. (2001). Nonreplicating persistence of *Mycobacterium tuberculosis*. *Annu Rev Microbiol* **55**, 139–163.

Weinstein, E. A., Yano, T., Li, L.-S., Avarbock, D., Avarbock, A., Helm, D., McColm, A. A., Duncan, K., Lonsdale, J. T. & Rubin, H. (2005). Inhibitors of type II NADH : menaquinone oxidoreductase represent a class of antitubercular drugs. *Proc Natl Acad Sci U S A* **102**, 4548–4553.

Yu, B. J., Sung, B. H., Lee, J. Y., Son, S. H., Kim, M. S. & Kim, S. C. (2006). *sucAB* and *sucCD* are mutually essential genes in *Escherichia coli*. *FEMS Microbiol Lett* **254**, 245–250.

Zomorrodi, A. R., Suthers, P. F., Ranganathan, S. & Maranas, C. D. (2012). Mathematical optimization applications in metabolic networks. *Metab Eng* **14**, 672–686.

Edited by: D. Kelly